

Journal of Materials Chemistry A

Unveiling π-π interactions in triptycene-phenazine/SWCNT redox chemistry using ESR spectroscopy

Journal:	Journal of Materials Chemistry A
Manuscript ID	TA-ART-06-2024-004176.R1
Article Type:	Paper
Date Submitted by the Author:	01-Aug-2024
Complete List of Authors:	Chen, Qi; Nagoya University, Department of Chemistry Suizu, Rie; Nagoya University, Department of Chemistry Shuku, Yoshiaki; Nagoya University, Omachi, Haruka; Nagoya University, Research Center for Materials Science Matsushita, Michio M.; Nagoya University Fukuura, Shuta; Kyoto Institute of Technology, Department of Chemistry and Materials Technology Yumura, Takashi; Kyoto Institute of Technology, Department of Chemistry and Materials Technology Bandow, Shunji; Meijo university, Appleied chemstry Awaga, Kunio; Nagoya University, Department of Chemistry

SCHOLARONE™ Manuscripts

ARTICLE

Unveiling π - π interactions in triptycene-phenazine/SWCNT redox chemistry using ESR spectroscopy

Qi Chen,^a Rie Suizu,^a Yoshiaki Shuku,^a Haruka Omachi,^a Michio M. Matsushita,^a Shuta Fukuura,^c Takashi Yumura,^c Shunji Bandow^b and Kunio Awaga*^a

Received 00th January 20xx, Accepted 00th January 20xx

DOI: 10.1039/x0xx000000x

Grasping the intricate π - π interactions between redox-active organic materials and conductive carbons is key to optimizing the performance of organic electrodes in energy storage devices. However, their precise role in redox chemistry remains elusive. In this work, the geometric congruence between the triptycene-phenazine (Trip-Phz) molecule, with its paddle-wheel structure, and the curved single-walled carbon nanotubes (SWCNTs), enable the self-assembly of Trip-Phz/SWCNT composites for aqueous supercapacitors. The Trip-Phz/SWCNT composites demonstrate well-defined redox peaks on cyclic voltammograms, coupled with a specific capacitance of 410 F/g. Our study goes one step further by capturing the electrochemically induced radicals through electron spin resonance (ESR) spectroscopy. The theoretically predicted robust π - π interactions between the inner-layer Trip-PhzH₆³⁺⁺ radicals and SWCNTs facilitate the electron transfer effect, leading to an ESR silent state. Conversely, the ESR spectra of the outer-layer radicals feature a Dysonian line, attributive of the high conductivity of the Trip-Phz/SWCNT composites (~10² S/cm). The insights gained from this research inspire the design of stable organic/carbon electrodes for advanced energy storage devices.

1. Introduction

Over the past decades, there has been growing interest in the potential of redox-active organic materials featuring unsaturated π -bonds, nitroxide radicals, quinone, and phenazine moieties. $^{1-3}$ These compounds are being explored as organic electrode materials (OEMs) for use in electrochemical energy storage devices, due to their intrinsic advantages of earth-abundant constituents, tunable physical properties, and versatility across various batteries. $^{3-5}$ Noteworthy is that, compared to inorganic counterparts, OEMs offer a remarkable theoretical capacity derived from complex multielectron redox reactions, positioning them as a promising alternative for advanced energy storage applications.

Nevertheless, the practical applications of OEMs currently grapples with two main challenges: high solubility that engenders the shuttle effect, and inherently poor electrical conductivity. To address the solubility issue, researchers have recommended various synthetic strategies for constructing large molecules by methods such as functional group substitution, 1D polymerization, and 2D organic framework engineering that includes covalent-organic frameworks and metal-organic frameworks. 6-8 These strategies have proven successful in bolstering the cycling stability of OEMs in metal-

ion batteries by minimizing their dissolution. Regarding the latter issue of poor electrical conductivity, a direct approach is the development of OEMs endowed with fully π -conjugated network; only a few such OEMs have achieved high conductivity to date. While more commonly, the objective is accomplished by blending highly conductive carbon materials, like carbon black or graphene, into the electrode composites to improve overall conductivity and mitigate solubility concerns.

Intriguingly, OEMs depend more on carbon substrates compared to transition-metal oxides. 10 The types of carbon additives can significantly influence the electrochemical stability and kinetics of OEMs. Carbons with sp^2 hybridization, such as SWCNTs and graphene, prove to be more effective in supporting OEMs than amorphous carbons due to their extended π -electron systems, establishing noncovalent combination with other π -electron systems, particularly aromatic molecules, through $\pi-\pi$ interactions. 11 In the solid-state electrochemistry, these interactions facilitate reversible redox processes and securely anchor the OEMs onto the surface of sp^2 carbons. 12,13

Although the concept of π - π interactions is acknowledged, their experimental characterization remains scant. While some Raman spectroscopic studies have hinted at their presence, yet these studies have focused on the pristine states of OEMs, disregarding the crucial impact these interactions have on redox chemistry within OEMs. 13,14 Unveiling these interactions is paramount for optimizing electrochemical performance. Furthermore, the intensity of these interactions is believed to be tightly correlates with the geometric matching between aromatic molecules and carbon substrates.

^a Department of Chemistry, Nagoya University, Furo-cho, Chikusa-ku, Nagoya, Aichi 464-8602, Japan.

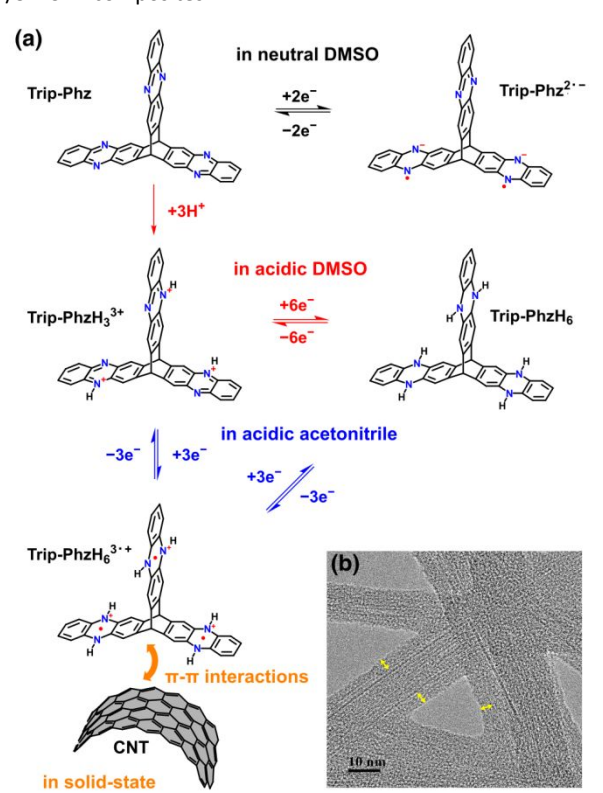
b. Department of Applied Chemistry, Meijo University, 1-501 Shiogamaguchi, Tenpaku-ku, Nagoya, Aichi 468-8502, Japan.

^c Faculty of Materials Science and Engineering, Graduate School of Science and Technology, Kyoto Institute of Technology, Matsugasaki, Sakyo-ku, Kyoto 606-8585. Japan.

[†]Supplementary Information available: [Synthesis and TEM of Trip-Phz/SWCNT composite, additional electrochemical results, magnetic properties]. See DOI: 10.1039/x0xx00000x

Research indicates that 2D graphene architectures offer stronger bonds with planar aromatic molecules, causing detectable shifts in Raman spectroscopy. 15,16 To our knowledge, this is the first ESR study aiming directly at elucidating the 3D $\pi-\pi$ interactions between a non-planar triptycene derivative and curved SWCNTs. $^{17-19}$

In our previous work, we synthesized a phenazine-fused triptycene acceptor known as Trip-Phz. Within its crystal structure, Trip-Phz forms a honeycomb network with wide 1D channels that are covered by $\pi\text{-electrons.}^{20}$ Moreover, we have also demonstrated that Trip-Phz molecules selectively adsorb onto the surface of SWCNT bundles, establishing a substantial 5 to 10 nm thick layer, and result in a hard and stable gelation of SWCNTs when they are mechanically mixed with Trip-Phz and organic solvents under ultrasonication (S1 in SI). Inspired by the promising stability and conductivity of the Trip-Phz/SWCNT composites, this study explores their redox chemistry in depth, along with theoretical studies on the specific affinity between Trip-Phz and SWCNTs. Significantly, ESR spectroscopy has provided concrete evidence of robust $\pi\text{-}\pi$ interactions within the reduced Trip-Phz/SWCNT composites.



Scheme 1 (a) Molecular structure of Trip-Phz, its redox reactions in different solvents (DMSO, acidic DMSO and acidic acetonitrile), and the possible electron transfer between reduced Trip-Phz and SWCNT. (b) TEM image of Trip-Phz/SWCNT composite, with the Trip-Phz layers marked by arrows for clarity.²¹

2. Results and discussion

2.1 Cyclic voltammogram of Trip-Phz solution

Phenazine derivatives are garnering attention as promising materials for energy storage, particularly due to their theoretical capacity for a two-electron reaction, which leads to the formation of dihydrophenazine compounds. Research, however, highlight that the redox

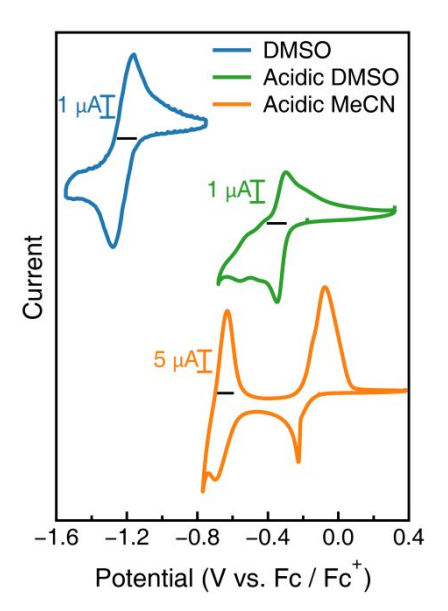


Fig. 1 Cyclic voltammogram (CV) of various saturated Trip-Phz solutions: Dimethyl sulfoxide (DMSO), DMSO with 0.2 M ptoluenesulfonic (PTS) acid (acidic DMSO), and acetonitrile with 0.2M PTS acid (acidic MeCN). Each of these solutions contains 0.1 M tetrabutylammonium perchlorate (TBAP) as a support electrolyte. The hypothesized redox reactions of Trip-Phz in these electrolytes are depicted in Scheme 1a.

reaction of phenazines is strongly influenced by both solvent and acidity.^{22,23} Similarly, the number of charge transfer during Trip-Phz redox reactions significantly depends on the electrolyte composition (Fig. 1). The ferrocenium/ferrocene (Fc+/Fc) redox couple was uased as a reference for potential calibration in each electrolyte (Figs. S4-6). In a neutral DMSO case, our previous studies have revealed that Trip-Phz undergoes a reversible redox reaction with a half-wave potential $(E_{1/2})$ of -1.22 V against Fc/Fc⁺.²⁰ This suggests the doping of two electrons into the doubly degenerated LUMO of Trip-Phz. In an acidic DMSO case, the protonated form (Trip-PhzH₃³⁺) exhibits three reversible waves at -0.32, -0.43, and -0.53 V, indicating an enhanced electronic coupling between the three phenazine moieties, which results in the lifting of the LUMO degeneracy. The possible sixelectron redox reaction is shown in Scheme 1a. When examining acidic acetonitrile (MeCN) with 0.2 M PTS acid, the first threeelectron wave shifts toward a more positive potential of -0.15 V ascribed to Lewis-type donor-acceptor interactions.²⁴ The apparent distortion of redox peaks could point to the instability of the reduced Trip-Phz radical cation (Trip-PhzH₆^{3•+}), potentially susceptible to oxygen attack or disproportionation reaction.²² Furthermore, the occurrence of a subsequent wave at -0.66 V represents another three-electron reaction, corresponding to the reduction of Trip-PhzH₆³*+ to Trip-PhzH₆.

2.2 Solid-state electrochemistry in Trip-Phz/SWCNT composites

Sonication of SWCNT bundles in a Trip-Phz/benzene dispersion resulted in the formation of a self-assembled Trip-Phz layer on the SWCNT surface, as confirmed by TEM image shown in Scheme 1b and Fig. S2. Control experiments involving triptycene (Trip) and phenazine (Phz) individually mixed with SWCNTs revealed no comparable molecular layer formation (Fig. S1). These findings

Journal Name ARTICLE

strongly suggest that the geometric complementarity between the paddle-wheel structure of Trip-Phz and the curved SWCNT surface drives the formation of Trip-Phz/SWCNT composites through robust $\pi\text{--}\pi$ interactions.

To delve deeper into the solid-state electrochemical processes within Trip-Phz/SWCNT composites, we implemented a sonication-assisted self-assembly method to prepare five samples, labeled Samples 1–5. These samples, differentiated by their varying Trip-Phz to SWCNTs weight ratios (1/5, 3/5, 5/5, 7/5, and 10/5), served as binder-free working electrodes. Their performance was assessed in an aqueous supercapacitor (proton half-cell) using a three-electrode setup, comprising a 1M H_2SO_4 electrolyte, a Pt wire as the counter electrode, and an Ag/AgCl electrode as the reference.

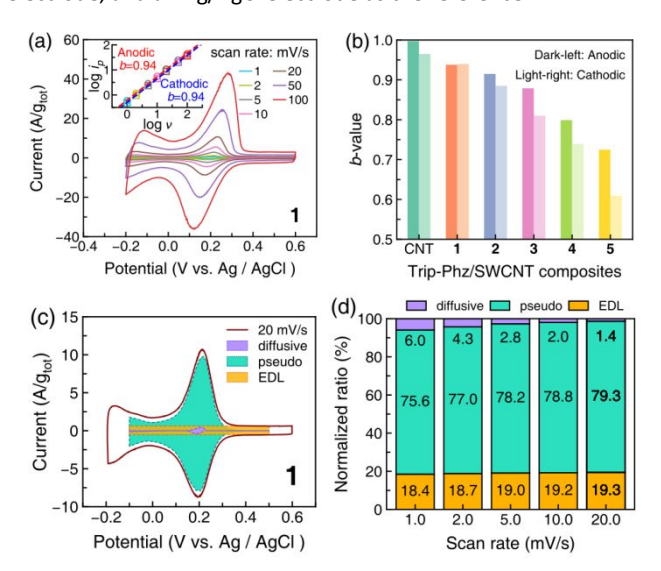


Fig. 2 Charge storage mechanism of Trip-Phz/SWCNT composites. (a) CV curves of Sample ${\bf 1}$ at various scan rates. The obtained b values are shown in the inset, showcasing log i_p plotted against log v. (b) Distribution of b values for all composites during both anodic and cathodic scans. (c) Decomposition of the compensated CV curve for Sample ${\bf 1}$ into three components. (d) The normalized ratios of the EDL, pseudo-capacitive, and diffusive contributions.

Fig. 2a illustrates the cyclic voltammetry for Sample 1 at various scan rates (1-100 mV/s). Here, a pair of reversible redox peaks is observed at $E_{1/2}$ =0.20 V (vs. Ag/AgCl), aligning with the proposed three-electron reaction of protonated Trip-Phz in the solid-state case (Scheme 1). An additional redox couple appears at potentials below 0.0 V, yet the operable potential window is constrained to value above -0.177 V vs. Ag/AgCl due to the onset of water splitting. As depicted for Samples 2 to 5 (Fig. S7), the current intensity of these redox peaks increases progressively, indicative of enhanced participation of Trip-Phz molecules within the redox processes with increasing compound content. The dependence of peak current i_p on scan rate v in CV curves is commonly described by a power law: i_0 = av^b . Notably, Sample 1 exhibits a b-value of 0.94 (Fig. 2a inset), suggesting dominance of a surface-controlled process. This is attributed to the thin layer of Trip-Phz facilitating rapid proton diffusion. Conversely, Sample 5, with a b-value of 0.61 (Fig. 2b), signifies a shift towards a diffusion-controlled behavior attributed to the ticker Trip-Phz layer hinders proton diffusion.

For a detailed understanding of the charge storage mechanism, comprehensive CV analyses were conducted. Compensation of parasitic resistance (Ohmic losses) and residual currents during scan direction reversals was achieved using reported method (Fig. S8).²⁵ Decomposing the compensated current (i) reveals three distinct current components: physical (diffusive) capacitive current ($k_{dl} \nu$), pseudo-capacitive current (k_1v) , and diffusive current $(k_2v^{1/2})$, as illustrated in Fig. 2c. The dominant diffusive current within the 0.4-0.6 V segment facilitates the determination of the $k_{\rm dl}$ component, arising from non-faradaic surface absorption of protons by the electric double-layer (EDL) of the SWCNT scaffold. The values of k_1 and k_2 could be determined by linear fitting of $(i - k_{\rm dl}v)/v^{1/2}$ and $v^{1/2}$ across whole potential range (Fig. S8). At a scan rate of 20 mV/s for Sample 1 (Fig. 2d, and see Fig. S9 for others), the identified contributions from these components are 28 F/g (EDL), 115 F/g (pseudo) and 3 F/g (diffusive) F/g. The substantial pseudocapacitance contribution signifies the rapid charge transfer kinetics between Trip-PhzH₃3+ and Trip-PhzH₆3•+, likely facilitated by robust π - π interactions with the SWCNTs. This hypothesis is further supported by the minimal charge transfer impedance observed in electrochemical impedance spectroscopy (EIS) (Fig. S10). With an increase in Trip-Phz content from Samples 1 to 5, both the proportion of diffusive capacitance and the charge transfer impedance rise, presumably due to weakened π - π interactions in the outer Trip-Phz layer.

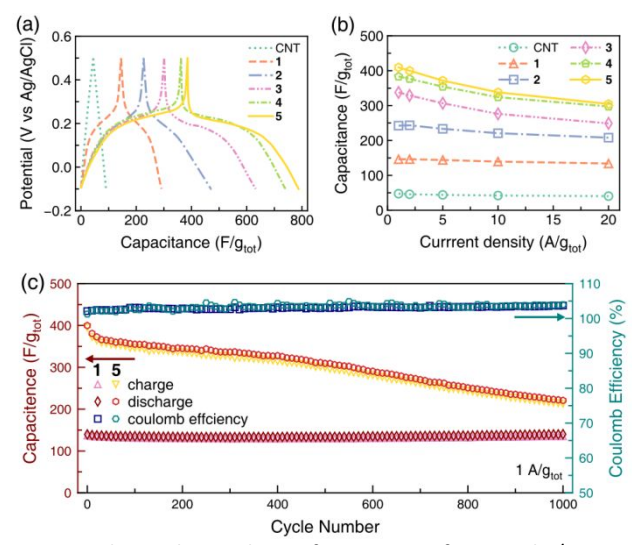


Fig. 3 Electrochemical performance of Trip-Phz/SWCNT composites. (a) The charge-discharge profiles for the bare SWCNTs and Samples **1–5** at a current density of 1 A g⁻¹. (b) The rate performance of the SWCNTs and Samples **1–5**, with specific capacitances and current densities normalized to the total weight of the composites. (c) The long-term cycling of Samples **1** and **5** as measured at 1 A/g.

Galvanostatic charge/discharge (GCD) tests were further conducted to evaluate the specific capacitance and cycling stability of Trip-Phz/SWCNT composites (Figs. 3 and S11). The bare SWCNTs electrode exhibits a limited specific capacitance of only 46 F/g (Fig. 3a). However, Sample 1 demonstrates a significant enhancement in specific capacitance, reaching 146 F/g_{tot}, with the Trip-Phz layer onle delivering a capacitance of 118 F/g_{tot} or 710 F/g_{Trip-Phz}, deduced by subtracting the EDL capacitance (constituting $^{\sim}$ 19% as depicted in Fig.

2d). This represents a significant 82% of its theoretical specific capacitance (861.6 F/g) calculated for the proposed three-electron reaction. The subsequent samples follow a progressive increase in specific capacitances, peaking at an impressive 410 F/g_{tot} for Sample 5. Fig. 3b highlights the superior rate performance of Sample 1 compared to other composites, attributed to its robust $\pi-\pi$ interactions. Sample 1 retains 87% of its capacitance even upon a current density increasing to 20 A/g. Conversely, Sample 5 shows a lower retention rate of 64%. Cycling stabilities Samples 1 and 5, cycled for 1000 cycles at 1 A/g_{tot} (Fig. 3c), reveal that Sample 1 maintains outstanding stability, retaining 99% of its initial capacitance after completing 1000 cycles. In contrast, Sample 5 preserves only 53% of its initial capacitance, indicating the poorer rate and cyclic performance likely due to weaker $\pi-\pi$ interactions within the outer Trip-Phz layer of Sample 5.

2.3 Theoretical calculation

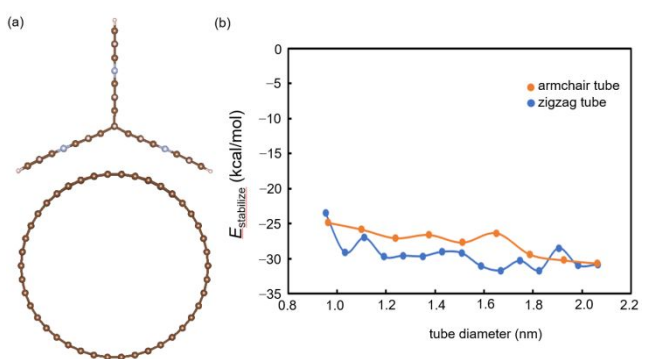


Fig. 4 (a) A representative optimized structure for Trip-Phz on SWCNT (Trip-Phz/(21,0) tube). (b) Changes of $E_{\text{stabilize}}$ values as a function of the tube diameter. Negative $E_{\text{stabilize}}$ values indicate that Trip-Phz/SWCNT composites are energetically stable relative to the dissociation limit toward Trip-Phz and SWCNT.

The key to the electrochemical performance of Trip-Phz/SWCNT composites would be interactions between Trip-Phz and SWCNTs, because such interactions are responsible for the immobilizing of Trip-Phz onto SWCNT, which prevents their dissolution. To elucidate interactions between a Trip-Phz and SWCNT, dispersion-corrected density functional theory (DFT) calculations with the PBE-D3 functional were conducted. Details of the DFT settings are shown in the Supporting Information. Given that the inner layer of Trip-Phz exhibits strong π - π interactions, a monolayer of Trip-Phz on SWCNT was considered to simplify the calculations. Optimized structures for Trip-Phz on an achiral SWCNT whose diameter ranges from 0.95 to 2.05 nm were obtained. Then, their stabilization energies ($E_{\text{stabilize}}$) were evaluated by comparing the dissociation limit toward Tri-Phz and SWCNT. Their representative optimized structure is displayed in Fig. 4(a). In Fig. 4(b), the changes in $E_{\text{stabilize}}$ as a function of the diameters of zigzag and armchair SWCNT are indicated by orange and blue lines, respectively. Negative $E_{\text{stabilize}}$ values, around -25 to -30kcal/mol, are seen in Fig. 4(b), indicating attractive long-range interactions operated in the optimized structures for Trip-Phz on SWCNT. Among the optimized structures, Trip-Phz on (21,0) SWCNT is the most stable, whose $E_{\text{stabilize}}$ value is -31.7 kcal/mol. Switching the dispersion corrections from D3 to D2 has almost unchanged the

E_{stabilize} value for the Trip-Phz and (21,0) SWCNT interaction, because the PBE-D2 value was calculated to be -31.1 kcal/mol. The origin of the attractive long-range interactions was further clarified by looking at the interatomic separations between Trip-Phz and (21,0) SWCNT in the optimized structure with the most significant $E_{\text{stabilize}}$ value. A detailed discussion can be found in Fig. S12. Briefly, Fig. S12 found counts of sp² carbon-atom separations between Trip-Phz and SWCNT in the region where attractive π - π interactions operate between benzene and naphthalene. Furthermore, similar analyses were performed for phenazine (Phz) or triptycene (Trip) on SWCNT, as shown in Fig. S13. The analyses showed that the $E_{\text{stabilize}}$ values for the Trip/SWCNT and Phz/SWCNT were less than half of that for Trip-Phz/SWCNT. The comparative analyses suggest that the paddlewheel structure of Trip-Phz is important to enhance attractive π - π interactions for stabilizing the nanocomposites, because Trip-Phz can perfectly align the curved sp² surface of SWCNT, rather than a simple planar Phz and a wheel Trip having smaller paddles.

2.4 Electron spin resonance

Electron spin resonance (ESR) spectroscopy is an exceptional technique that directly probes unpaired electrons. Moreover, ESR stands out unique ability to distinguish the unpaired electrons between organic free radicals (localized spins), itinerant electrons (metal)^{26,27}, and polarons (semiconductor)²⁸, by detecting their distinct effective *g*-factors, which are influenced by spin-orbit coupling, spin-spin interaction, and local coordination environments. Furthermore, high sensitivity of ESR spectroscopy allows the precise determination of spin concentrations even at trace levels. Despite its capabilities, there is a lack of direct ESR evidence to support $\pi-\pi$ interactions and associated electron transfer between redox-active molecules and SWCNTs, which are through to underpin the superior electrochemical performance of organic/SWCNT electrodes.

In light of this, we employed continuous-wave ESR spectroscopy to monitor the spin states of Trip-PHz/SWCNT composites, aiming to gain insights into their redox chemistry. The ESR spectrum of pristine SWCNTs exhibits a broad ferromagnetic resonance, likely stemming from residual catalyst particles (Fig. S19). ²⁹ As SWCNTs have Luttinger liquid behavior, it has been confirmed that no radical signal would be detected due to the itinerant electrons in SWCNTs causing a broadening beyond ESR's detectable limits at room temperature. ³⁰ Additionally, the absence of a radical signal after self-assembly of neutral Trip-Phz onto the SWCNTs surface suggests that electron transfer in these pristine states is not easily observed.

Fig. 5a presents the ESR spectra of the composites after discharge to -0.1 V. Notably, both bare SWCNTs and Sample 1 exhibit no detectable radical signals, even after reduction. Moreover, the exsitu ESR spectra of Sample 1 have almost no change during the discharge from 0.5 to -0.1 V (Fig. S23), hinting at the absence of the Trip-PhzH₆^{3*+} radicals. This could be explained by the high electron affinity of SWCNT electronic bands, which are believed to act as efficient radical scavengers, as reported in previous studies. ^{31,32} The radicals electrochemically generated in Sample 1 are readily being scavenged by the SWCNTs through electron transfer effects. For Samples 2 to 5, featuring thicker Trip-Phz layers in comparison to Sample 1, we observed a distinct narrow radical signal in the ESR

Journal Name ARTICLE

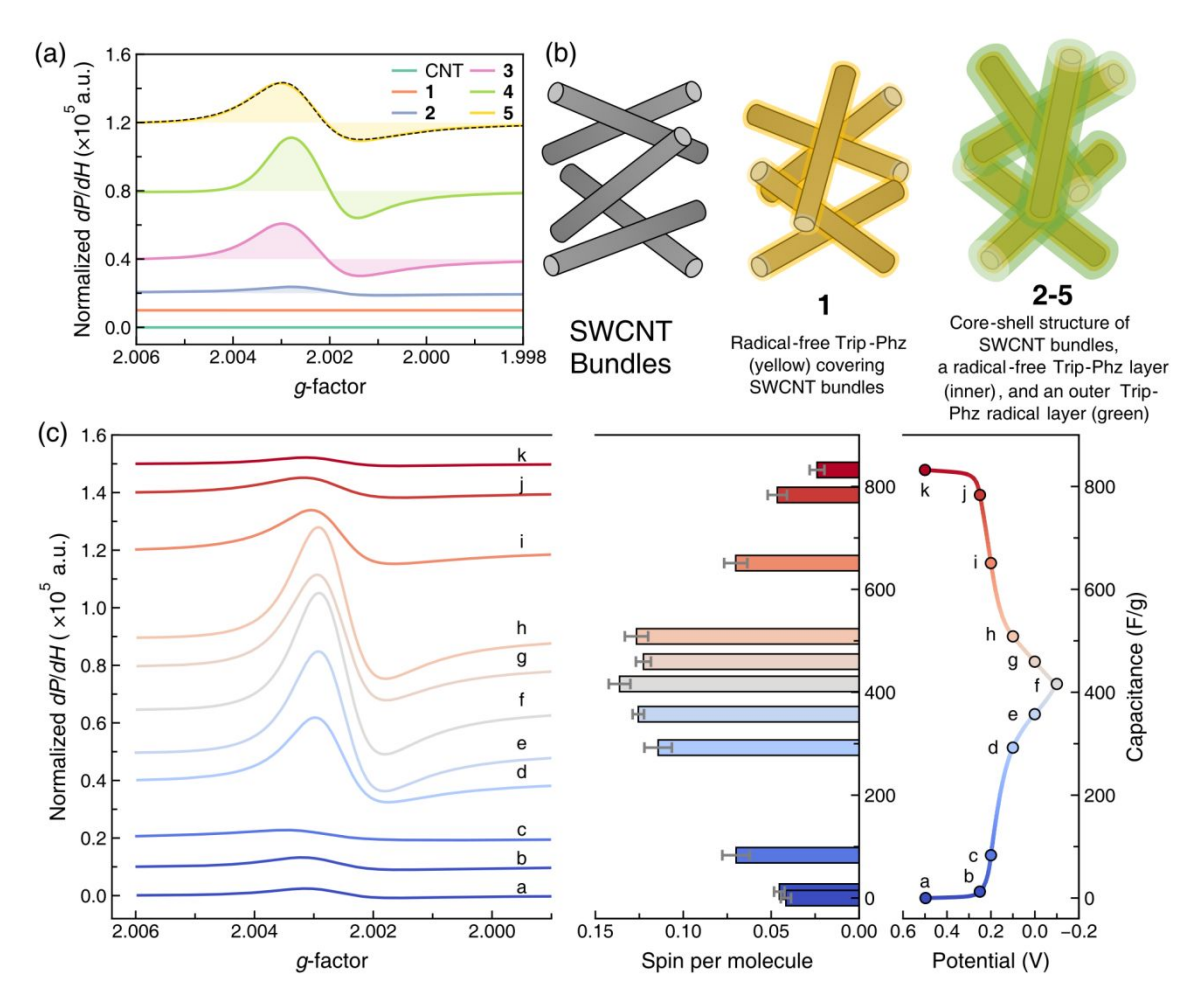


Fig. 5 Electron spin resonance (ESR) spectroscopy of reduced Trip-Phz/SWCNT composites. (a) ESR spectra of Trip-Phz/SWCNTs composites after discharge to -0.1V. The spectrum of Sample 5 is fitted with a Dysonian function (dashed line). (d) Schematic representations of SWCNTs bundles, electrochemically reduced Sample 1, and Samples 2–5 after reduction. (c) Ex-situ ESR spectra of Sample 5 at various states-of-charge (labeled a–f), aligning with points marked on the charge-discharge profile. ESR spectra are vertically offset for clarity. The calculated number of spins per Trip-Phz molecule is plotted against capacitance.

spectra (Fig. 5a). This difference could be assigned to two main factors: 1) the enhanced radical generation due to the thicker Trip-Phz layer, which could exceed the scavenging capacity of the SWCNTs, and 2), a shielding effect where the inner Trip-Phz layer may prevent outer radicals from being scavenged by SWCNTs due to weaker π – π interactions (as illustrated in Fig. S22).

The ESR spectra for Samples 2–5 interestingly show asymmetrical Dysonian lines (Figs. 5a and S19). Representative fitting with the Dysonian function (dashed lines) matches well with the observed spectra, 33 with parameters indicating a g-factor of 2.0028(2), a peak-to-peak width (ΔH_{pp}) of 0.24 mT, and an asymmetry parameter (A/B) of 2.4. These Dysonian signature are likely the result of the skin effect, which arises from the high conductivity of the SWCNT scaffold (Fig. S14). 34 The thickness of Trip-Phz/SWCNT electrode might surpass the skin depth, $\delta = c/\sqrt{2\pi\omega\sigma}$. 35 For instance, the conductivity of Sample 5 (50 S/cm, Fig. S16) derived an estimated skin depth of ~70 µm, whereas the thickness of electrode is ~100 µm (the conductivity of Sample 1 is shown in Fig. S15 and Table S2). This hypothesis is further supported by observing a symmetric Lorentzian lineshape for the radical signal when a thinner film electrode (~10 µm) was employed (Fig. S20).

In quantifying the spin concentration, we calibrated against a well-known nitroxide radical reference (TEMPOL), which establishes a relationship between the number of spins and the double integral of the ESR intensity (Fig. 2).³⁶ The calculated spin concentration shows a slight decline across Sample **2** to **5** (29%, 21%, 17%, 14%, normalized by Trip-Phz, Tabel S4). This lower-than-expected spin concentration, despite a reduction of Trip-PhzH₃³⁺ to Trip-PhzH₆³⁺⁺, can also be attributed to the radical scavenging and skin effect. Namely, ESR's limited penetration depth may only allow us to probe a subset of the existing radical spins (Fig. 5b).

We conducted ex-situ ESR spectroscopy Sample **5** to gain deeper insights into the intricacies of the redox mechanism within Trip-Phz/SWCNT composites (Fig. 5c). Cycling a single electrode through a series of potential points (a–k) results in significant and reversible changes in the ESR spectra, confirming the reversible generation and oxidation of the Trip-PhzH₆³⁺⁺ radical species. All ESR spectra display Dysonian lineshape, signifying the highly conductive nature of Trip-Phz/SWCNT composites throughout the redox reactions. The linear increase/decrease in spin concentration during discharge/charge (middle of Fig. 5c) implies that the reduction from Trip-PhzH₃³⁺ to Trip-PhzH₆³⁺⁺ occurs, with no further reduction to Trip-PhzH₆ down

to -0.1 V. It should be noted that both inner and outer Trip-Phz are reduced at the same time, the spin concentration would be expected to remain constant if radical scavenging was done for the inner Trip-Phz. The temperature-independent behaviors observed in the SQUID (Figs. S17, S18) and ESR (Figs. S25, S26) susceptibility indicate the delocalization of unpaired electrons within the Trip-Phz/SWCNT composites. With the high electrical conductivity (~10² S/cm), skin effect, temperature-independent paramagnetism, and electron transfer induced radical scavenging, all these observations emphasize robust $\pi-\pi$ interactions within Trip-Phz/SWCNT composites. These $\pi-\pi$ interactions facilitate the charge transfer kinetics and improve the stability of redox processes between Trip-PhzH3³+ and Trip-PhzH6³+, making Trip-Phz/SWCNT composites a promising electrode material in energy storage devices.

3. Conclusions

This study provides an in-depth understanding of the redox chemistry in Trip-Phz/SWCNT composites, integrating insights from both solution and solid-state electrochemistry, as well as ESR spectroscopy. Leveraging the unique π - π interactions, supported by DFT calculations and TEM imaging, Trip-Phz molecules self-assemble on SWCNTs to form a composite structure, unlike triptycene or phenazine which exhibit negligible absorption. Our CV and GCD studies reveal a captivating three-electron reaction of Trip-Phz in protic electrolytes, namely, a reversible conversion between the Trip- $PhzH_3^{3+}$ protonated cation and the Trip-Phz $H_6^{3\bullet+}$ radical cation. Interestingly, as the Trip-Phz content increases from Samples 1 to 5, thin-layer Trip-Phz displays rapid change transfer kinetics and a pseudo-capacitive mechanism for charge storage, likely driven by robust π – π interactions. This interaction significantly enhances the rate and cycling performance of the composite. For thick Trip-Phz layer, the redox processes seem to be controlled by proton diffusion, as indicated by the decomposition of CV curves and EIS results. Furthermore, the ex-situ ESR spectra provides solid evidence of a radical-involved redox reaction and the π - π interactions. The reduced Sample 1 does not show a detectable radical signal, suggesting an effective radical scavenging by the SWCNT scaffold. Meanwhile, the Dysonian lines observed in Samples 2-5 point towards the formation of Trip-PhzH₆³*+ radicals, highlighting the significant electrical conductivity within these composites. These spectroscopic findings offer strong evidence of the impact of π - $\boldsymbol{\pi}$ interactions between the inner Trip-Phz layers and the SWCNTs, which are essential in governing the redox chemistry of the composites. These insights pave the way for further development of organic/carbon composites for advanced energy storage systems and controllable CNT-based electronics. The conclusions section should come in this section at the end of the article, before the acknowledgements.

Author contributions

Qi Chen: data curation, methodology, conceptualization, formal analysis, writing – original draft, writing – review & editing. Rie Suizu: conceptualization, methodology, investigation. Yoshiaki Shuku: data

curation, methodology. Haruka Omachi: methodology. Michio. M Matsushita: data curation. Shuta Fukuura: DFT calculation, writing – original draft. Takashi Yumura: DFT calculation, writing – review & editing, Shunji Bandow: conceptualization, methodology, formal analysis. Kunio Awaga: conceptualization, funding acquisition, project administration, resources, supervision, writing – review & editing.

Conflicts of interest

There are no conflicts to declare.

Data availability

The data supporting this article have been included as part of the Supplementary Information.

Acknowledgements

The authors acknowledge the Japan Society for the Promotion of Science (JSPS) KAKENHI Grants 20H02707 (to R.S.) and 20H05621 (to K.A.), and the Japan Science and Technology Agency (JST) PRESTO Grant JPMJPR21A9 (to R.S.) for funding this work.

Notes and references

- 1 Y. Lu and J. Chen, *Nat. Rev. Chem.*, 2020, **4**, 127–142.
- D. Xu, M. Liang, S. Qi, W. Sun, L. P. Lv, F. H. Du,
 B. Wang, S. Chen, Y. Wang and Y. Yu, ACS Nano,
 2021, 15, 47–80.
- 3 S. Lee, J. Hong and K. Kang, *Adv. Energy Mater.*, 2020, **10**, 2001445.
- 4 H. Lyu, X. G. Sun and S. Dai, *Adv. Energy Sustainability Res.*, 2021, **2**, 2000044.
- T. B. Schon, B. T. McAllister, P. F. Li and D. S.
 Seferos, *Chem. Soc. Rev.*, 2016, 45, 6345–6404.
- 6 S. Legoupy, E. Lebègue and C. Cougnon, *Electrochem. Commun.*, 2016, **70**, 47–50.
- W. da Silva, A. C. Queiroz and C. M. A. Brett, *Electrochim. Acta*, 2020, **347**, 136284.
- 8 Y. Kou, Y. Xu, Z. Guo and D. Jiang, *Angew. Chem.*, 2011, **123**, 8912–8916.

Journal Name ARTICLE

- 9 K. Lee, S. Cho, H. P. Sung, A. J. Heeger, C. W. Lee and S. H. Lee, *Nature*, 2006, **441**, 65–68.
- C. Peng, G. H. Ning, J. Su, G. Zhong, W. Tang, B. Tian, C. Su, Di. Yu, L. Zu, J. Yang, M. F. Ng, Y. S. Hu, Y. Yang, M. Armand and K. P. Loh, *Nat. Energy*, 2017, 2, 17074.
- 11 J. M. Smalley, R. E. Banerjee and S. Wong, *J. Am. Chem. Soc*, 2003, **128**, 5114–5118.
- H. Ito, T. Murata, M. Fujisaki, R. Tsuji and Y.
 Morita, *ChemSusChem*, 2021, **14**, 1377–1387.
- 13 M. Lee, J. Hong, H. Kim, H. D. Lim, S. B. Cho, K. Kang and C. B. Park, *Adv. Mater.*, 2014, **26**, 2558–2565.
- D. Xu, Z. Cao, Z. Ye, H. Zhang, L. Wang, M. John,
 P. Dong, S. Gao, J. Shen and M. Ye, *Chem. Eng. J*,
 2021, 417, 129245.
- 15 X. F. Zhang and X. Shao, *J. Photochem. Photobiol. A: Chem.*, 2014, **278**, 69–74.
- 16 F. Tournus, S. Latil, M. I. Heggie and J. C. Charlier, *Phys. Rev. B*, 2005, **72**, 075431.
- S. X. L. Luo, C. J. Lin, K. H. Ku, K. Yoshinaga and T.
 M. Swager, ACS Nano, 2020, 14, 7297–7307.
- 18 S. Selmani and D. J. Schipper, *Angew. Chem. Int. Ed.*, 2018, **57**, 2399–2403.
- P. Hammershøj, P. H. H. Bomans, R. Lakshminarayanan, J. Fock, S. H. Jensen, T. S. Jespersen, T. Brock-Nannestad, T. Hassenkam, J. Nygård, N. A. J. M. Sommerdijk, K. Kilså, T. Bjørnholm and J. B. Christensen, *Chem. Eur. J.*, 2012, **18**, 8716–8723.
- 20 R. Ushiroguchi, Y. Shuku, R. Suizu and K. Awaga, *Cryst. Growth Des.*, 2020, **20**, 7593–7597.
- 21 R. Ushiroguchi, R. Suizu, Y. Matsunaga, H. Omachi, Y. Doi, Y. Masubuchi, S. Bandow and K. Awaga, *Chem. Lett.*, 2022, **51**, 1070–1073.

- D. T. Sawyer and R. Y. Komai, *Anal. Chem.*, 1972,44, 715–721.
- 23 M. N. Jackson, S. Oh, C. J. Kaminsky, S. B. Chu, G. Zhang, J. T. Miller and Y. Surendranath, *J. Am. Chem. Soc.*, 2018, **140**, 1004–1010.
- 24 G. Gritzner, *J. Phys. Chem.*, 1986, **90**, 5478–5485.
- X. Pu, D. Zhao, C. Fu, Z. Chen, S. Cao, C. Wang and Y. Cao, *Angew. Chem. Int. Ed.*, 2021, **60**, 21310–21318.
- 26 K. P. Dinse, J. van Tol, A. Ozarowski and B. Corzilius, *Appl. Magn. Reson.*, 2010, **37**, 595–603.
- 27 M. Havlicek, W. Jantsch, Z. Wilamowski, K. Yanagi, H. Kataura, M. H. Rümmeli, H. Malissa, A. Tyryshkin, S. Lyon, A. Chernov and H. Kuzmany, *Phys. Rev. B*, 2012, **86**, 045402.
- 28 K. Mizoguchi, M. Nechtschein, J.-P. Travers and C. Menardo, *Phys. Rev. Lett.*, 1989, **63**, 66–69.
- V. Likodimos, S. Glenis, N. Guskos and C. L. Lin, *Phys. Rev. B*, 2007, **76**, 075420.
- 30 B. Dóra, M. Gulácsi, J. Koltai, V. Zólyomi, J. Kürti and F. Simon, *Phys. Rev. Lett.*, 2008, **101**, 106408.
- 31 I. Fenoglio, M. Tomatis, D. Lison, J. Muller, A. Fonseca, J. B. Nagy and B. Fubini, *Free Radic. Biol. Med.*, 2006, **40**, 1227–1233.
- 32 A. Martínez and A. Galano, *J. Phys. Chem. C*, 2010, **114**, 8184–8191.
- 33 F. J. Dysont, *Phys. Rev.*, 1958, **98**, 349–359.
- M. Havlicek, W. Jantsch, Z. Wilamowski, K. Yanagi, H. Kataura, M. H. Rümmeli, H. Malissa, A. Tyryshkin, S. Lyon, A. Chernov and H. Kuzmany, *Phys. Rev. B*, 2012, **86**, 045402.

- 35 P. Petit, E. Jouguelet, J. E. Fischer, A. G. Rinzler and R. E. Smalley, *Phys. Rev. B*, 1997, **56**, 9275–9278.
- 36 Q. Chen, O. Adeniran, Z. F. Liu, Z. Zhang and K. Awaga, *J. Am. Chem. Soc.*, 2023, **145**, 1062–1071.

The data supporting this article have been included as part of the Supplementary Information.